One Tracer, Dual Platforms: Unlocking Versatility of Fluorescent Probes in TR-FRET and NanoBRET Target Engagement Assays

Erika Y. Monroy[1,2], Xin Yu[1,2], Dong Lu[1,2], Xiaoli Qi[1,2], Jin Wang [1,2,3,*]

[1]*Verna and Marrs McLean Department of Biochemistry and Molecular Pharmacology, Baylor College of Medicine, Houston, Texas 77030, United States*

[2]*Center for NextGen Therapeutics, Baylor College of Medicine, Houston, Texas 77030, United States*

[3]*Department of Molecular and Cellular Biology, Baylor College of Medicine, Houston, Texas 77030, United States*

*Correspondence: wangj@bcm.edu

Abstract: Target engagement assays are critical for drug discovery, with Time-Resolved Fluorescence Resonance Energy Transfer (TR-FRET) and Nano Bioluminescence Resonance Energy Transfer (NanoBRET) representing two complementary approaches for biochemical and cellular evaluation. Traditionally, these platforms demand distinct fluorescent tracers tailored to their unique detection systems, requiring separate probe development for comprehensive target characterization. Despite their widespread adoption, the development of platform-specific fluorescent tracers often leads to increased costs and experimental complexity. In this study, two fluorescent tracers, T2- BODIPY -FL and T2-BODIPY-589, initially developed for receptor-interacting protein kinase 1 (RIPK1) target engagement studies in TR-FRET and NanoBRET applications respectively, were systematically evaluated for their performance across both platforms under various detection parameters. By evaluating their performance across both assay systems, we demonstrate that both tracers can effectively bridge biochemical and cellular assays, delivering reliable measurements. T2-BODIPY-589, with its red-shifted spectral properties, exhibits superior performance in NanoBRET assays (Z' up to 0.80) while maintaining acceptable functionality in TR-FRET systems (Z'=0.53). In contrast, T2-BODIPY -FL provides optimal performance for TR-FRET (Z'=0.57) but also demonstrates potential for use in NanoBRET (Z' up to 0.72), albeit with reduced efficiency. Competition assays with an unlabeled inhibitor yielded consistent binding constants across all tracer-platform combinations, validating their reliability for quantitative measurements. Our findings highlight the potential for integrating a single tracer across diverse assay platforms, reducing the need for separate probe development and enhancing experimental consistency. This approach has broad implications for streamlining assay development, improving data comparability, and enables more direct comparisons between biochemical and cellular data, with broader implications for integrated drug discovery programs across diverse target classes.

Keywords: *Fluorescent tracer, TR-FRET, NanoBRET, target engagement, high-throughput screen, Z' factor, RIPK1*

INTRODUCTION

Over the past few decades, biomedical research has accelerated significantly due to rapid advancements in biochemical, cellular, and tissue-based assays. These developments have expedited the discovery and development of new therapeutics by elucidating crucial protein-protein interactions that lead to more effective treatment strategies.[1,2] While several methods exist for measuring direct interactions between targets and compounds—including surface plasmon resonance, thermal shift assays, nuclear magnetic resonance, and various calorimetry techniques—many suffer from limitations such as low throughput, requirements for purified proteins, limited sensitivity, or high noise levels.[3–6]

Fluorescence/luminescence-based technologies have emerged as critical tools in modern molecular biology and drug discovery. Fluorescent/luminescence-based assays have become prevalent in high-throughput screening due to their numerous advantages: high sensitivity, signal stability, adaptability across different assay formats, operational simplicity, and non-destructive analysis capabilities.[7–10] Their versatility has made them indispensable across scientific disciplines, from detecting viral proteins in infected cells to screening diverse compound libraries against challenging therapeutic targets.[11,12]

Among the diverse applications of fluorescence/luminescence-based technology, two techniques have gained particular prominence: Time-Resolved Fluorescent Resonance Energy Transfer (TR-FRET) and Nano Bioluminescent Resonance Energy Transfer (NanoBRET). Both methods have become mainstays over the past decade in measuring protein-ligand interactions in drug discovery, offering noninvasive detection with high sensitivity and low background noise. As a result, they have both gained increasing popularity in preclinical biomedical research. [13–16]

TR-FRET combines the sensitivity of fluorescence with the specificity of FRET to study molecular interactions. This technique relies on energy transfer between a donor—typically a lanthanide chelate—and an acceptor fluorophore when they are in close proximity (1-10 nm) (Figure 1A).[17] What distinguishes TR-FRET is its use of donor fluorophores with exceptionally long fluorescent lifetimes (microseconds), enabling time-resolved detection that significantly reduces background fluorescence and enhances signal-to-noise ratios.[17–19] TR-FRET assays allow quantitative measurements of protein-ligand interactions that can be seamlessly integrated into high-throughput screening platforms for drug discovery.[20–24]

NanoBRET, developed by researchers at Promega Corporation, represents a significant advancement in monitoring molecular interactions within cellular environments.[25] This innovative technique leverages bioluminescent resonance energy transfer to observe target-ligand interactions in real time under physiologically relevant conditions.[26] At the heart of the NanoBRET system is NanoLuc, a compact 19 kDa luciferase enzyme that functions as a light-emitting donor.[27] When NanoLuc catalyzes its substrate furimazine, it generates a bioluminescent signal that can excite nearby acceptor fluorophores positioned within the critical 1-10 nm proximity range required for efficient energy transfer (Figure 1B). Unlike TR-FRET, which depends on external illumination to initiate the energy transfer process, NanoBRET's spontaneous light generation through enzymatic catalysis eliminates several common technical challenges. This self-contained light production system minimizes the autofluorescence and photobleaching issues that often plague fluorescence-based methods, and significantly reduces background noise. The technique has established itself as an

invaluable research tool for tracking molecular interactions as they occur within the complex environment of living cells, providing researchers with unprecedented insights into the dynamics of target engagement by small molecules and biologics under conditions that closely mirror the native cellular context.[28–33]

Fluorescent tracers serve as crucial components in both TR-FRET and NanoBRET assays, though their spectral requirements differ significantly between platforms.[34] In Terbium-based TR-FRET assays, fluorophores that absorb at 488 nm are typically selected for tracer development, leveraging the characteristic emission bands of the lanthanide donor.[35–37] Conversely, NanoBRET assays commonly utilize red-shifted fluorophores such as BODIPY-589 or NCT derivatives as acceptors, chosen specifically for their minimal spectral overlap with NanoLuc donor emission, which optimizes energy transfer efficiency while reducing background signal. Throughout typical drug discovery campaigns, researchers frequently require both TR-FRET and NanoBRET platforms to comprehensively characterize compound-target interactions from biochemical to cellular contexts. This dual requirement traditionally necessitates the synthesis of separate tracers conjugated with platform-specific fluorophores, increasing both development costs and potential variability between assay formats.

In this study, we explore an innovative approach by evaluating the cross-platform compatibility of tracers originally designed for a single assay type. Specifically, we assess whether a TR-FRET-optimized tracer can function effectively in NanoBRET applications and vice versa. Using two fluorescent tracers, T2-BODIPY-FL (T2-BDP-FL) and T2-BODIPY-589 (T2-BDP-589), which were initially developed for RIPK1 target engagement studies, we systematically characterize their performance across both platforms under various detection parameters and assay conditions.[10,24,38,39] These molecules serve as excellent models for demonstrating versatility across biochemical and cellular assay formats. Through comprehensive comparative analysis, demonstrate that thoughtfully designed fluorescent tracers can successfully bridge the gap between in vitro and cellular assay systems, delivering consistent and biologically relevant data while streamlining the tracer development process for multi-platform applications in drug discovery.

RESULTS

Key Considerations in Assay Development, Optimization and Validation for High-Throughput Screening

The development, optimization, validation, and analysis of assays to assess performance metrics are critical prerequisites for the efficient evaluation of new chemical entities in diverse screening methodologies. These foundational steps have been extensively documented in the literature.[40–42] Prior to full-scale screening, assays must undergo rigorous validation, beginning with the optimization of the dynamic range of signal response and variability. The assessment of assay performance using hit confirmation criteria has been extensively studied by Zhang and colleagues and is summarized in Table 1.[43] One of the most widely adopted assay quality metrics is the Z’ factor, which accounts for both the amplitude and variability of positive and negative responses. This metric is universally used to determine the suitability of an assay for high-throughput screening (HTS).[44] However, while the signal window and Z’ factor measurements are effective for optimizing assay dynamic range and initial parameters, they are not suitable for evaluating concentration-response assays. This must be

followed by characterizing the reproducibility of key pharmacological parameters, such as IC□□, EC□□, and K□, in concentration-response assays using well-characterized reference compounds.

Photophysical characterization

To facilitate comprehensive target engagement studies across both biochemical and cellular platforms, we previously developed two specialized fluorescent tracers: T2-BDP-FL (Figure 1C) for TR-FRET applications and T2-BDP-589 (Figure 1D) for NanoBRET assays.[10]

In TR-FRET assays, terbium (Tb) represents an ideal donor due to its exceptional photophysical properties, most notably its long fluorescence lifetime (milliseconds rather than nanoseconds) that enables time-gated detection and significantly improved signal-to-noise ratios.[36,45,46] Upon excitation at 340 nm, Tb exhibits four major emission transitions from its $^5D_4$ excited state to various ^7F_J ground states (J = 6, 5, 4, 3), producing characteristic narrow emission bands at approximately 490, 548, 587, and 620 nm. The first transition ($^5D_4 \rightarrow {}^7F_6$) at 490 nm provides an excellent spectral overlap with the absorption spectrum of T2-BDP-FL (Figure 2A), making this donor-acceptor pair highly efficient for energy transfer. Conventional TR-FRET assays utilizing this pair typically employ 520 ± 10/490 ± 10 nm filter settings, which capture the T2-BDP-FL emission while effectively discriminating against the terbium signal.

Interestingly, the second ($^5D_4 \rightarrow {}^7F_5$ at 548 nm) and third ($^5D_4 \rightarrow {}^7F_4$ at 587 nm) transitions of terbium demonstrate considerable overlap with the absorption spectrum of T2-BDP-589, despite this fluorophore being primarily designed for NanoBRET applications (Figure 2B).[47,48] This spectral compatibility suggests potential versatility of T2- BDP-589 in TR-FRET assays, can be optimized using alternative filter settings such as 640 ± 10/490 ± 10 nm or 640 ± 10/550 ± 25 nm to capture the red-shifted emission of T2-BDP-589 while maintaining discrimination against the terbium signal.

In NanoBRET assays, the NanoLuc luciferase generates a blue luminescent signal with an emission maximum at 460 nm that gradually tapers to approximately 600 nm.[49,50] The absorption spectrum of T2-BDP-FL shows significant overlap with this NanoLuc emission profile (Figure 4A), theoretically enabling energy transfer in cellular systems. However, this spectral proximity creates potential challenges with signal bleed-through, where the intense donor signal may contaminate the acceptor channel. To address this concern, we systematically evaluated various emission settings using a linear variable filter (LVF) monochromator detector (520 ± 30 nm, 550 ± 30 nm, and 580 ± 30 nm) and a 610 nm long-pass filter to identify optimal detection parameters that maximize the T2-BDP-FL signal while minimizing NanoLuc bleed-through. Similarly, we assessed the performance of T2-BDP-589 (Figure 4B), which was specifically designed with red-shifted spectral properties to provide greater separation from the NanoLuc emission and potentially reduce signal interference in cellular assays.

Through this comprehensive characterization of the photophysical properties of both tracers across multiple detection parameters, we sought to determine whether these fluorescent tracers could demonstrate unexpected versatility across both TR-FRET and NanoBRET platforms, potentially simplifying assay development and providing greater experimental flexibility in target engagement studies.

Optimizing TR-FRET Filter Pairs for RIPK1 with Fluorescent Tracers

To evaluate the cross-platform compatibility of our fluorescent tracers, we optimized TR-FRET assay conditions using T2-BDP-FL and T2-BDP-589 with His-tagged RIPK1 and an anti-6xHis-Tb antibody.

Three filter pair combinations (520 ± 10 nm/490 ± 10 nm, 640 ± 10 nm/490 ± 10 nm, and 640 ± 10 nm/550 ± 25 nm) were tested to determine optimal detection parameters.

Our results, summarized in Table 2, revealed distinct performance profiles for each tracer. T2-BDP-FL exhibited optimal performance with the 520 ± 10 nm/490 ± 10 nm filter pair (Z' = 0.57, signal window = 6.0), consistent with its spectral properties and TR-FRET compatibility. However, it performed poorly with other filter combinations, producing negative Z' values. Despite being designed primarily for NanoBRET applications, T2-BDP-589 demonstrated adequate TR-FRET performance with the 640 ± 10 nm/490 ± 10 nm filter pair (Z' = 0.53, signal window = 7.8) and acceptable performance with the 520 ± 10 nm/490 ± 10 nm filter pair (Z' = 0.40, signal window = 10.5), while its performance with the 640 ± 10 nm/550 ± 25 nm filter pair was marginal (Z' = 0.29, signal window = 3.1).

Dose-response analysis in Figure 2C and 2D confirmed the functionality of both tracers in TR-FRET format, with T2-BDP-FL exhibiting an equilibrium dissociation constant (K_d) of 608 nM using the 520 ± 10 nm/490 ± 10 nm filter pair and T2-BDP-589 showing a K_d of 443 nM with the 640 ± 10 nm/490 ± 10 nm filter pair. Both tracers were effectively displaced by the unlabeled T2 inhibitor, demonstrating specific binding to RIPK1.

Although additional filters (520 ± 10 nm/490 ± 10 nm and 640 ± 10 nm/550 ± 25 nm) met minimal assay feasibility criteria, only conditions with Z' values exceeding 0.5 were deemed suitable for subsequent IC_{50} determination with unlabeled T2 inhibitor. This optimization process establishes a robust and sensitive TR-FRET assay for RIPK1, ensuring reliable characterization of binders.

TR-FRET assay for RIPK1 with Optimized Filter Settings for T2-BDP-FL and T2-BDP-589

In Figure 3 we applying optimized filter settings and assessed the relative affinity of an unlabeled T2 inhibitor, a highly selective RIPK1 inhibitor. To accurately determine the inhibitory constant (K_i), we selected fluorescent tracer concentrations at their K_d values using the Cheng-Prusoff equation ($K_i = IC_{50}/2$).[51] Interestingly, competition assays with the unlabeled T2 inhibitor (Table 3) yielded K_i values of 18 ± 0.70 nM for T2-BDP-FL and 54 ± 5.9 nM for T2-BDP-589. This discrepancy likely arises from differences in detection parameters rather than true binding affinity variations, as filter settings capture distinct emission regions, affecting signal intensity and calculated binding metrics.

While the T2-BDP-589 probe allows for two possible filter settings, the T2-BDP-FL filter settings (520 ± 10 nm/490 ± 10 nm) are better aligned with the emission spectrum of the TR-FRET assay and provide a more sensitive measure of unlabeled T2 inhibitory activity, ensuring greater consistency across experiments. These findings confirm that while T2-BDP-FL remains the optimal choice for TR-FRET applications, T2-BDP-589 demonstrates versatility and potential for cross-platform use with appropriate detection parameters.

Optimizing NanoBRET Assay Conditions for Accurate RIPK1 Target Engagement Measurement with Fluorescent Tracers

To assess the versatility of our fluorescent tracers in cellular contexts, we systematically evaluated both T2-BDP-FL and T2-BDP-589 in NanoBRET assays using NanoLuc-tagged RIPK1 expressed in HEK293T cells. We employed a linear variable filter (LVF) monochromator detector to investigate various emission combinations, allowing us to establish optimal detection parameters. The monochromator was incrementally adjusted at 30 nm bandwidth intervals to select a continuous range of wavelengths, allowing for more flexible and precise adjustments during experiments.

T2-BDP-589, designed for NanoBRET applications, demonstrated strong performance across various emission pairs using the LVF monochromator and appropriate filters. The highest Z' factor of 0.80 and a signal window of 15 were achieved with the 610 nm long-pass filter and the 460 ± 30 nm monochromator setting. The combination of the 610 ± 30 nm and 460 ± 30 nm settings yielded a Z' factor of 0.79 and a signal window of 17. In contrast, the 640 ± 30 nm and 460 ± 30 nm combination resulted in a Z' factor of 0.58 and a signal window of 7.7. Additionally, the performance with the 580 ± 30 nm and 460 ± 30 nm setting yielded a Z' factor of 0.62 and a signal window of 7.6. These results confirm that T2-BDP-589 is well-suited for NanoBRET applications, exhibiting robust assay performance across multiple detection parameters.

Despite being optimized for TR-FRET, T2-BDP-FL also demonstrated effective NanoBRET compatibility, particularly with the 520 ± 30 nm and 460 ± 30 nm monochromator settings (Z' = 0.72, signal window = 14). However, a notable decline in performance was observed with the 610 nm long-pass filter and the 460 ± 30 nm monochromator setting, which resulted in a Z' factor of 0.21 and a signal window of 3.1, likely due to insufficient emission from T2-BDP-FL at longer wavelengths.

Dose-response analysis provided further insights into the tracers' binding affinities. T2-BDP-589 exhibited K_d values ranging from 232 nM to 267 nM across different monochromator and filter combinations (Figures 4F-H), demonstrating strong and specific binding characteristics. In contrast, T2-BDP-FL displayed slightly higher K_d values, ranging from 619 nM to 711 nM (Figures 4C-E).

While both tracers exhibited reduced performance when shifting the acceptor wavelength, T2-BDP-589 maintained superior overall reliability, and better assay performance. These optimizations are essential for ensuring accurate quantification of target engagement, ultimately facilitating more reliable and reproducible NanoBRET assay results.

NanoBRET assay for RIPK1 with Optimized Monochromator and Filter Settings

Competition assays with the unlabeled T2 inhibitor (Figure 5, Table 5) yielded consistent K_i values across all monochromator and filter combinations, ranging from 6.6 ± 1.6 nM to 14 ± 2.5 nM. Notably, there was minimal variation in the K_i values obtained with different tracers or detection settings, indicating robust and reliable assay performance regardless of the specific monochromator and filter configurations. These findings demonstrate that both tracers exhibit remarkable versatility in NanoBRET assays when appropriate wavelength combinations are selected. While T2-BDP-589 performs optimally in this format as expected, including lower probe concentrations required for effective target engagement, enhanced signal specificity, reduced risk of inner-filter effects, and minimal probe-induced cytotoxicity that could otherwise interfere with normal cellular functions, the unexpected effectiveness of T2-BDP-FL in NanoBRET applications highlights the potential for using a single tracer across multiple assay platforms, simplifying assay development and facilitating direct comparison of biochemical and cellular data.

DISCUSSION

Our systematic evaluation of T2-BDP-FL and T2-BDP-589 across TR-FRET and NanoBRET platforms reveals unexpected versatility in these fluorescent tracers, challenging the conventional approach of developing platform-specific probes.

Both TR-FRET and NanoBRET assays were employed to determine the binding affinities of a T2 inhibitor against RIPK1, a target of interest in therapeutic research. In TR-FRET assays, T2-BDP-FL

exhibited a K_d of 608 nM (Z’ = 0.57, signal window = 6.0) with 520 ± 10 nm/490 ± 10 nm filter pair, while T2-BDP-589 demonstrated a slightly lower K_d of 443 nM (Z’ = 0.53, signal window = 7.8) with 640 ± 10 nm/490 ± 10 nm filter pair, suggesting that the latter may exhibit a higher affinity for the target under the optimized conditions for TR-FRET. However, the variation in K_d values may be attributed to differences in filter settings rather than actual differences in binding affinity, highlighting the influence of assay parameters on data interpretation. Competition assays with an unlabeled T2 inhibitor yielded different K_i values: 18 ± 0.70 nM for T2-BDP-FL and 54 ± 5.9 nM for T2-BDP-589. This discrepancy is likely due to differences in detection parameters rather than true binding affinity variations.

In NanoBRET assays, both T2-BDP-FL and T2-BDP-589 demonstrated strong binding to RIPK1, with T2-BDP-589 outperforming T2-BDP-FL with the highest Z’ factor (0.80) and signal window (15) observed using the 610 nm long-pass filter and 460 ± 30 nm monochromator setting. This improved performance in NanoBRET assays can be attributed to the greater spectral separation between NanoLuc and T2-BDP-589, which reduces the risk of inner-filter effects and signal bleed-through, ensuring more reliable data. Surprisingly, T2-BDP-FL also showed effective NanoBRET compatibility, particularly with the 520 ± 30 nm and 460 ± 30 nm monochromator setting (Z' = 0.72, signal window = 14). However, its performance declined with longer wavelengths. Notably, the similar K_i values (6.6-14 nM) obtained across multiple monochromator and filter combinations for T2-BDP-589 and T2-BDP-FL confirmed their suitability for quantitative target engagement studies.

T2-BDP-FL offers higher quantum yield and established performance in conventional TR-FRET assays, making it excellent for biochemical screening.[52] However, its shorter emission wavelength increases susceptibility to interference from autofluorescent compounds.

T2-BDP-589, with its red-shifted spectral properties, provides superior resistance to interference from autofluorescent compounds and cellular components. This advantage is particularly valuable when screening compound libraries that may contain fluorescent molecules or when working in complex biological matrices. The longer emission wavelength (589 nm) provides greater separation from both terbium and NanoLuc emissions, reducing signal bleed-through and improving signal-to-background ratios.

We recommend T2-BDP-589 as the preferred tracer for integrated assay development across both platforms. Its adequate functionality in TR-FRET, excellent performance in NanoBRET, and red-shifted spectral properties that minimize interference from autofluorescent compounds make it the more versatile choice for comprehensive target engagement studies. For laboratories focused exclusively on TR-FRET screening without cellular validation, T2-BDP-FL remains an excellent choice.

The demonstrated cross-platform compatibility of these fluorescent tracers represents a significant advancement with far-reaching implications for assay development in drug discovery. This approach fundamentally challenges the conventional wisdom that different assay platforms necessarily require different tracers, potentially streamlining probe development while reducing associated costs and complexity. By enabling the use of identical tracers across both biochemical and cellular formats, researchers can make more direct, reliable comparisons between in vitro and cellular data without introducing tracer-specific variables that might otherwise confound interpretation. The principles established in this study have broad applicability beyond kinases, potentially extending to diverse target classes including membrane receptors, nuclear receptors, and protein-protein interactions

where consistent target engagement measurements across platforms would provide valuable insights. Furthermore, this methodology establishes a foundation for developing sophisticated multiplexed assays capable of simultaneously monitoring interactions with multiple targets, offering a more comprehensive view of compound selectivity and engagement profiles within a single experimental framework.

In conclusion, our evaluation demonstrates that carefully designed fluorescent tracers can effectively function across both biochemical and cellular assay platforms. By selecting tracers with appropriate spectral properties, particularly those with red-shifted emission profiles like T2-BDP-589, researchers can streamline assay development, reduce experimental variability, and obtain more consistent target engagement data across experimental systems.

ASSOCIATED CONTENT

The Supporting Information is available free of charge at (). Characterization data and biological assay procedures.

AUTHOR INFORMATION

Corresponding Author

Jin Wang – *Department of Biochemistry and Molecular Pharmacology and Department of Molecular and Cellular Biology, Baylor College of Medicine, Houston, Texas 77030, United States;*

Email: wangj@bcm.edu

Author Contributions

E.Y.M. and J.W. designed the experiments. E.Y.M performed the experiments X.Y. and D.L. provided fluorescent tracers. E.Y.M. X.Q. and J.W. wrote the manuscript.

Competing Interest Statement

J.W. is the co-founder of Chemical Biology Probes LLC. J. W. has stock ownership in CoRegen Inc and serves as a consultant for this company. J.W. is the co-founder of Fortitude Biomedicines, Inc. and holds equity interest in this company.

ACKNOWLEDGEMENT

The research was supported in part by National Institute of Health (R01-CA268518 and R01-CA250503 to J.W.), Cancer Prevention & Research institute of Texas (CPRIT, RP220480 to J.W.), and the Michael E. DeBakey, M.D., Professorship in Pharmacology to J.W. We also acknowledge Dr. Mazitschek and BMG Labtech's advice and assistance with the customized filters.

ABBREVIATIONS

TR-FRET, Time-Resolved Fluorescence Resonance Energy Transfer; NanoBRET, Nano Bioluminescence Resonance Energy Transfer; NanoLuc, NanoLuc luciferase; RIPK1, receptor-interacting protein kinase 1; HEK293T, human embryonic kidney 293T cells; K_d, equilibrium dissociation constant; K_i, inhibition constant; Z', Z-prime factor; LP, longpass filter; BODIPY, dipyrrometheneboron difluoride; Tb, terbium; FL, fluorescein; NCT, nonchloro TOM; IC_{50}, half-maximal inhibitory concentration; EC_{50}, half-maximal effective concentration; mM, millimolar; nm, nanometer; µM, micromolar; nM, nanomolar

REFERENCES

(1) Nada, H.; Choi, Y.; Kim, S.; Jeong, K. S.; Meanwell, N. A.; Lee, K. New Insights into Protein–Protein Interaction Modulators in Drug Discovery and Therapeutic Advance. *Signal Transduct. Target. Ther.* **2024**, *9*, 341. https://doi.org/10.1038/s41392-024-02036-3.

(2) Nada, H.; Choi, Y.; Kim, S.; Jeong, K. S.; Meanwell, N. A.; Lee, K. New Insights into Protein–Protein Interaction Modulators in Drug Discovery and Therapeutic Advance. *Signal Transduct. Target. Ther.* **2024**, *9* (1), 1–32. https://doi.org/10.1038/s41392-024-02036-3.

(3) Murali, S.; Rustandi, R. R.; Zheng, X.; Payne, A.; Shang, L. Applications of Surface Plasmon Resonance and Biolayer Interferometry for Virus–Ligand Binding. *Viruses* **2022**, *14* (4), 717. https://doi.org/10.3390/v14040717.

(4) Qi, C.; Mankinen, O.; Telkki, V.-V.; Hilty, C. Measuring Protein–Ligand Binding by Hyperpolarized Ultrafast NMR. *J. Am. Chem. Soc.* **2024**, *146* (8), 5063–5066. https://doi.org/10.1021/jacs.3c14359.

(5) Author, N. *Exploring Optimal Interaction Techniques | SPR vs ITC vs MST vs BLI* |. Nicoya - Improving Human Life by Helping Scientists Succeed. https://nicoyalife.com/blog/spr-vs-itc-vs-mst-vs-bli/ (accessed 2025-03-20).

(6) Jarmoskaite, I.; AlSadhan, I.; Vaidyanathan, P. P.; Herschlag, D. How to Measure and Evaluate Binding Affinities. *eLife* **2020**, *9*, e57264. https://doi.org/10.7554/eLife.57264.

(7) Wegner, K. D.; Jin, Z.; Lindén, S.; Jennings, T. L.; Hildebrandt, N. Quantum-Dot-Based Förster Resonance Energy Transfer Immunoassay for Sensitive Clinical Diagnostics of Low-Volume Serum Samples. *ACS Nano* **2013**, *7* (8), 7411–7419. https://doi.org/10.1021/nn403253y.

(8) Blay, V.; Tolani, B.; Ho, S. P.; Arkin, M. R. High-Throughput Screening: Today's Biochemical and Cell-Based Approaches. *Drug Discov. Today* **2020**, *25* (10), 1807–1821. https://doi.org/10.1016/j.drudis.2020.07.024.

(9) Busby, S. A.; Carbonneau, S.; Concannon, J.; Dumelin, C. E.; Lee, Y.; Numao, S.; Renaud, N.; Smith, T. M.; Auld, D. S. Advancements in Assay Technologies and Strategies to Enable Drug Discovery. *ACS Chem. Biol.* **2020**, *15* (10), 2636–2648. https://doi.org/10.1021/acschembio.0c00495.

(10) Yu, X.; Lin, H.; Li, F.; Wang, J.; Lu, D. Development of Biochemical and Cellular Probes to Study RIPK1 Target Engagement. *ACS Med. Chem. Lett.* **2024**, *15* (6), 906–916. https://doi.org/10.1021/acsmedchemlett.4c00104.

(11) Gorshkov, K.; Morales Vasquez, D.; Chiem, K.; Ye, C.; Nguyen Tran, B.; Carlos de la Torre, J.; Moran, T.; Chen, C. Z.; Martinez-Sobrido, L.; Zheng, W. SARS-CoV-2 Nucleocapsid Protein TR-FRET Assay Amenable to High Throughput Screening. *ACS Pharmacol. Transl. Sci.* **2022**, *5* (1), 8–19. https://doi.org/10.1021/acsptsci.1c00182.

(12) Larson, J. E.; Hardy, P. B.; Schomburg, N. K.; Wang, X.; Kireev, D.; Rossman, K. L.; Pearce, K. H. Development of a High-Throughput TR-FRET Screening Assay for a Fast-Cycling KRAS Mutant. *SLAS Discov.* **2023**, *28* (1), 39–47. https://doi.org/10.1016/j.slasd.2022.12.001.

(13) Abdel-Rahman, S. A.; Zhang, L.; Gabr, M. T. Development of a High-Throughput TR-FRET Screening Assay for LAG-3/FGL1 Interaction. *SLAS Discov.* **2023**, *28* (4), 188–192. https://doi.org/10.1016/j.slasd.2023.04.003.

(14) O'Neill, K.; Lyons, S. K.; Gallagher, W. M.; Curran, K. M.; Byrne, A. T. Bioluminescent Imaging: A Critical Tool in Pre-Clinical Oncology Research. *J. Pathol.* **2010**, *220* (3), 317–327. https://doi.org/10.1002/path.2656.

(15) Yu, X.; Wang, J. Chapter Nine - Quantitative Measurement of PROTAC Intracellular Accumulation. In *Methods in Enzymology*; Burslem, G. L., Ed.; Targeted Protein Degradation; Academic Press, 2023; Vol. 681, pp 189–214. https://doi.org/10.1016/bs.mie.2022.11.001.

(16) Lin, H.; Riching, K.; Lai, M. P.; Lu, D.; Cheng, R.; Qi, X.; Wang, J. Lysineless HiBiT and NanoLuc Tagging Systems as Alternative Tools for Monitoring Targeted Protein Degradation. *ACS Med. Chem. Lett.* **2024**, *15* (8), 1367–1375. https://doi.org/10.1021/acsmedchemlett.4c00271.

(17) Cho, U.; Chen, J. K. Lanthanide-Based Optical Probes of Biological Systems. *Cell Chem. Biol.* **2020**, *27* (8), 921–936. https://doi.org/10.1016/j.chembiol.2020.07.009.

(18) Degorce, F. HTRF: A Technology Tailored for Drug Discovery - A Review of Theoretical Aspects and Recent Applications. *Curr. Chem. Genomics* **2009**, *3* (1), 22–32. https://doi.org/10.2174/1875397300903010022.

(19) Algar, W. R.; Hildebrandt, N.; Vogel, S. S.; Medintz, I. L. FRET as a Biomolecular Research Tool — Understanding Its Potential While Avoiding Pitfalls. *Nat. Methods* **2019**, *16* (9), 815–829. https://doi.org/10.1038/s41592-019-0530-8.

(20) Rectenwald, J. M.; Hardy, P. B.; Norris-Drouin, J. L.; Cholensky, S. H.; James, L. I.; Frye, S. V.; Pearce, K. H. A General TR-FRET Assay Platform for High-Throughput Screening and Characterizing Inhibitors of Methyl-Lysine Reader Proteins. *SLAS Discov.* **2019**, *24* (6), 693–700. https://doi.org/10.1177/2472555219844569.

(21) Machleidt, T.; Robers, M. B.; Hermanson, S. B.; Dudek, J. M.; Bi, K. TR-FRET Cellular Assays for Interrogating Posttranslational Modifications of Histone H3. *J. Biomol. Screen.* **2011**, *16* (10), 1236–1246. https://doi.org/10.1177/1087057111422943.

(22) Wesley, N. A.; Skrajna, A.; Simmons, H. C.; Budziszewski, G. R.; Azzam, D. N.; Cesmat, A. P.; McGinty, R. K. Time Resolved-Fluorescence Resonance Energy Transfer Platform for Quantitative Nucleosome Binding and Footprinting. *Protein Sci.* **2022**, *31* (6), e4339. https://doi.org/10.1002/pro.4339.

(23) Greenway, H.; Wang, J. Evaluation of High-Affinity Monoclonal Antibodies and Antibody-Drug Conjugates by Homogenous Time-Resolved FRET. *ACS Med. Chem. Lett.* **2024**, *15* (9), 1598–1605. https://doi.org/10.1021/acsmedchemlett.4c00317.

(24) Lin, W.; Li, Y.; Min, J.; Liu, J.; Yang, L.; Lee, R. E.; Chen, T. Development of BODIPY FL Thalidomide As a High-Affinity Fluorescent Probe for Cereblon in a Time-Resolved Fluorescence Resonance Energy Transfer Assay. *Bioconjug. Chem.* **2020**, *31* (11), 2564–2575. https://doi.org/10.1021/acs.bioconjchem.0c00507.

(25) Machleidt, T.; Woodroofe, C. C.; Schwinn, M. K.; Méndez, J.; Robers, M. B.; Zimmerman, K.; Otto, P.; Daniels, D. L.; Kirkland, T. A.; Wood, K. V. NanoBRET—A Novel BRET Platform for the Analysis of Protein–Protein Interactions. *ACS Chem. Biol.* **2015**, *10* (8), 1797–1804. https://doi.org/10.1021/acschembio.5b00143.

(26) *A bioluminescence resonance energy transfer (BRET) system: Application to interacting circadian clock proteins*. https://doi.org/10.1073/pnas.96.1.151.

(27) Hall, M. P.; Unch, J.; Binkowski, B. F.; Valley, M. P.; Butler, B. L.; Wood, M. G.; Otto, P.; Zimmerman, K.; Vidugiris, G.; Machleidt, T.; Robers, M. B.; Benink, H. A.; Eggers, C. T.; Slater, M. R.; Meisenheimer, P. L.; Klaubert, D. H.; Fan, F.; Encell, L. P.; Wood, K. V. Engineered Luciferase Reporter from a Deep Sea Shrimp Utilizing a Novel Imidazopyrazinone Substrate. *ACS Chem. Biol.* **2012**, *7* (11), 1848–1857. https://doi.org/10.1021/cb3002478.

(28) Liu, Y.; Song, G.; Shao, X.-X.; Liu, Y.-L.; Guo, Z.-Y. Quantitative Measurement of Cell Membrane Receptor Internalization by the Nanoluciferase Reporter: Using the G Protein-Coupled Receptor RXFP3 as a Model. *Biochim. Biophys. Acta BBA - Biomembr.* **2015**, *1848* (2), 688–694. https://doi.org/10.1016/j.bbamem.2014.11.026.

(29) Lohse, M. J.; Nuber, S.; Hoffmann, C. Fluorescence/Bioluminescence Resonance Energy Transfer Techniques to Study G-Protein-Coupled Receptor Activation and Signaling. *Pharmacol. Rev.* **2012**, *64* (2), 299–336. https://doi.org/10.1124/pr.110.004309.

(30) *Recent progress in assays for GPCR drug discovery*. https://doi.org/10.1152/ajpcell.00464.2021.

(31) Mahan, S. D.; Riching, K. M.; Urh, M.; Daniels, D. L. Kinetic Detection of E3:PROTAC:Target Ternary Complexes Using NanoBRETNanoBRET Technology in Live Cells. In *Targeted Protein Degradation: Methods and Protocols*; Cacace, A. M., Hickey, C. M., Békés, M., Eds.; Springer US: New York, NY, 2021; pp 151–171. https://doi.org/10.1007/978-1-0716-1665-9_8.

(32) Robers, M. B.; Dart, M. L.; Woodroofe, C. C.; Zimprich, C. A.; Kirkland, T. A.; Machleidt, T.; Kupcho, K. R.; Levin, S.; Hartnett, J. R.; Zimmerman, K.; Niles, A. L.; Ohana, R. F.; Daniels, D. L.; Slater, M.; Wood, M. G.; Cong, M.; Cheng, Y.-Q.; Wood, K. V. Target Engagement and Drug Residence Time Can Be Observed in Living Cells with BRET. *Nat. Commun.* **2015**, *6* (1), 10091. https://doi.org/10.1038/ncomms10091.

(33) Robers, M. B.; Friedman-Ohana, R.; Huber, K. V. M.; Kilpatrick, L.; Vasta, J. D.; Berger, B.-T.; Chaudhry, C.; Hill, S.; Müller, S.; Knapp, S.; Wood, K. V. Quantifying Target Occupancy of Small Molecules Within Living Cells. *Annu. Rev. Biochem.* **2020**, *89* (Volume 89, 2020), 557–581. https://doi.org/10.1146/annurev-biochem-011420-092302.

(34) Dopfer, J.; Vasta, J. D.; Müller, S.; Knapp, S.; Robers, M. B.; Schwalm, M. P. tracerDB: A Crowdsourced Fluorescent Tracer Database for Target Engagement Analysis. *Nat. Commun.* **2024**, *15* (1), 5646. https://doi.org/10.1038/s41467-024-49896-5.

(35) Cho, U.; Riordan, D. P.; Ciepla, P.; Kocherlakota, K. S.; Chen, J. K.; Harbury, P. B. Ultrasensitive Optical Imaging with Lanthanide Lumiphores. *Nat. Chem. Biol.* **2018**, *14* (1), 15–21. https://doi.org/10.1038/nchembio.2513.

(36) Bünzli, J.-C. G. Lanthanide Luminescence for Biomedical Analyses and Imaging. *Chem. Rev.* **2010**, *110* (5), 2729–2755. https://doi.org/10.1021/cr900362e.

(37) Payne, N. C.; Kalyakina, A. S.; Singh, K.; Tye, M. A.; Mazitschek, R. Bright and Stable Luminescent Probes for Target Engagement Profiling in Live Cells. *Nat. Chem. Biol.* **2021**, *17* (11), 1168–1177. https://doi.org/10.1038/s41589-021-00877-5.

(38) Yu, X.; Lu, D.; Qi, X.; Paudel, R. R.; Lin, H.; Holloman, B. L.; Jin, F.; Xu, L.; Ding, L.; Peng, W.; Wang, M. C.; Chen, X.; Wang, J. Development of a RIPK1 Degrader to Enhance Antitumor Immunity. *Nat. Commun.* **2024**, *15* (1), 10683. https://doi.org/10.1038/s41467-024-55006-2.

(39) Vasta, J. D.; Corona, C. R.; Wilkinson, J.; Zimprich, C. A.; Hartnett, J. R.; Ingold, M. R.; Zimmerman, K.; Machleidt, T.; Kirkland, T. A.; Huwiler, K. G.; Ohana, R. F.; Slater, M.; Otto, P.; Cong, M.; Wells, C. I.; Berger, B.-T.; Hanke, T.; Glas, C.; Ding, K.; Drewry, D. H.; Huber, K. V. M.; Willson, T. M.; Knapp, S.; Müller, S.; Meisenheimer, P. L.; Fan, F.; Wood, K. V.; Robers, M. B. Quantitative, Wide-Spectrum Kinase Profiling in Live Cells for Assessing the Effect of Cellular ATP on Target Engagement. *Cell Chem. Biol.* **2018**, *25* (2), 206-214.e11. https://doi.org/10.1016/j.chembiol.2017.10.010.

(40) *Design of Signal Windows in High Throughput Screening Assays for Drug Discovery*. https://doi.org/10.1177/108705719700200306.

(41) Zhang, J.-H.; Chung, T. D. Y.; Oldenburg, K. R. A Simple Statistical Parameter for Use in Evaluation and Validation of High Throughput Screening Assays. *SLAS Discov.* **1999**, *4* (2), 67–73. https://doi.org/10.1177/108705719900400206.

(42) Taylor, P. B.; Stewart, F. P.; Dunnington, D. J.; Quinn, S. T.; Schulz, C. K.; Vaidya, K. S.; Kurali, E.; Lane, T. R.; Xiong, W. C.; Sherrill, T. P.; Snider, J. S.; Terpstra, N. D.; Hertzberg, R. P. Automated Assay Optimization with Integrated Statistics and Smart Robotics. *SLAS Discov.* **2000**, *5* (4), 213–225. https://doi.org/10.1177/108705710000500404.

(43) Zhang, J.-H.; Chung, T. D. Y.; Oldenburg, K. R. Confirmation of Primary Active Substances from High Throughput Screening of Chemical and Biological Populations: A Statistical Approach and Practical Considerations. *J. Comb. Chem.* **2000**, *2* (3), 258–265. https://doi.org/10.1021/cc9900706.

(44) *Requirements | European Lead Factory*. https://www.europeanleadfactory.eu/how-collaborate-us/information-programme-owners/requirements (accessed 2025-01-30).

(45) Lindén, S.; Kumar Singh, M.; David Wegner, K.; Regairaz, M.; Dautry, F.; Treussart, F.; Hildebrandt, N. Terbium-Based Time-Gated Förster Resonance Energy Transfer Imaging for Evaluating Protein–Protein Interactions on Cell Membranes. *Dalton Trans.* **2015**, *44* (11), 4994–5003. https://doi.org/10.1039/C4DT02884H.

(46) *Spectrum [BODIPY FL] | AAT Bioquest*. https://www.aatbio.com/fluorescence-excitation-emission-spectrum-graph-viewer/bodipy_fl (accessed 2025-03-10).

(47) *Spectrum [BODIPY™ 576/589] | AAT Bioquest*. https://www.aatbio.com/fluorescence-excitation-emission-spectrum-graph-viewer/bodipy_576_589 (accessed 2025-03-10).

(48) Golja, D. R.; Woldemariam, M. M.; Dejene, F. B.; Kim, J. Y. Photoluminescence Processes in τ-Phase Ba1.3Ca0.7-x-ySiO4:xDy3+/yTb3+ Phosphors for Solid-State Lighting. *R. Soc. Open Sci. 9* (6), 220101. https://doi.org/10.1098/rsos.220101.

(49) Dale, N. C.; Johnstone, E. K. M.; White, C. W.; Pfleger, K. D. G. NanoBRET: The Bright Future of Proximity-Based Assays. *Front. Bioeng. Biotechnol.* **2019**, *7*, 56. https://doi.org/10.3389/fbioe.2019.00056.

(50) *NanoBRET on Microplate Readers | BMG LABTECH*. https://www.bmglabtech.com/en/blog/nanobret/ (accessed 2025-03-10).

(51) Yung-Chi, C.; Prusoff, W. H. Relationship between the Inhibition Constant (*K*I) and the Concentration of Inhibitor Which Causes 50 per Cent Inhibition (*I*50) of an Enzymatic Reaction. *Biochem. Pharmacol.* **1973**, *22* (23), 3099–3108. https://doi.org/10.1016/0006-2952(73)90196-2.

(52) Kurata, S.; Kanagawa, T.; Yamada, K.; Torimura, M.; Yokomaku, T.; Kamagata, Y.; Kurane, R. Fluorescent Quenching-Based Quantitative Detection of Specific DNA/RNA Using a BODIPY® FL-Labeled Probe or Primer. *Nucleic Acids Res.* **2001**, *29* (6), e34. https://doi.org/10.1093/nar/29.6.e34.

List of Tables

Table 1. Criteria for Signal Window and Z' [a] 16

Table 2. Z' for TR-FRET Assay [a] 17

Table 3. Evaluation of RIPK1 Unlabeled T2 Inhibitor Binding Affinities in TR-FRET Assay with Varying Filter Conditions 18

Table 4. Z' for NanoBRET Assay [a] 19

Table 5. Evaluation of RIPK1 Unlabeled T2 Inhibitor Binding Affinities in NanoBRET Assay with Variable Monochromatic and Filter Conditions 20

Table 1. Criteria for Signal Window and Z' [a]

Signal Window	*Z'*
Recommended: SW > 2	**Excellent: Z' > 0.5**
Acceptable: SW > 1	**Do-able: 0 < Z' < 0.5**
Unacceptable: SW < 1	**Unacceptable: Z' < 0**

SW = signal window

[a] The Signal Window is classified into three categories: Recommended, which ensures optimal assay performance; Acceptable, which meets minimum quality requirements; and Unacceptable, which indicates poor assay conditions requiring optimization. The Z' factor is categorized as Excellent (> 0.5), indicating robust assay performance; Do-able (0 – 0.5), signifying moderate quality with potential for improvement; and Unacceptable (< 0), representing inadequate assay performance.

Table 2. Z' for TR-FRET Assay [a]

Probes	*Filter Settings*	*Maximum Signal*		*Background Signal*		*Z'*	*SW*
		Mean	*SD*	*Mean*	*SD*		
T2-BODIPY-FL	520 ± 10 nm/490 ± 10 nm	9.01×10^4	3930	4.89×10^4	1920	0.57	6.0
	640 ± 10 nm/490 ± 10 nm	2.00×10^4	417	1.94×10^4	142	-1.7	-2.5
	640 ± 10 nm/550 ± 25 nm	3.80×10^4	929	3.97×10^4	302	-1.2	-2.2
T2-BODIPY-589	520 ± 10 nm/490 ± 10 nm	1.80×10^4	141	2.17×10^4	589	0.40	10.5
	640 ± 10 nm/490 ± 10 nm	5.46×10^4	1030	3.94×10^4	1340	0.53	7.8
	640 ± 10 nm/550 ± 25 nm	1.22×10^5	2750	9.35×10^4	3950	0.29	3.1

[a] The optimized results in the Time-Resolved Fluorescent Resonance Energy Transfer (TR-FRET) assay were conducted at a probe concentration of 2 µM. The table summarizes the mean and standard deviation (SD) of the maximum signal and background for each fluorescent tracer, alongside the calculated Z' factor and signal window for various filter settings.

Table 3. Evaluation of RIPK1 Unlabeled T2 Inhibitor Binding Affinities in TR-FRET Assay with Varying Filter Conditions

Probes	*Filter Settings*	*T2 Inhibitor Ki (nM)*
T2-BODIPY-FL	520 ± 10 nm/490 ± 10 nm	18 ± 0.70
T2-BODIPY-589	640 ± 10 nm/490 ± 10 nm	54 ± 5.9

Table 4. Z' for NanoBRET Assay [a]

Probes	*Monochromatic Settings with Selected Filter*	*Maximum Signal*		*Background Signal*		*Z'*	*SW*
		Mean	*SD*	*Mean*	*SD*		
T2-BODIPY-FL	520 ± 30 nm/460 ± 30 nm	238	12.4	-8.95	10.3	0.72	14
	550 ± 30 nm/460 ± 30 nm	72.0	2.85	-0.40	5.24	0.66	17
	580 ± 30 nm/460 ± 30 nm	15.5	0.60	-0.30	1.28	0.64	17
	610 nm LP/460 ± 30 nm	13.6	1.00	-1.11	2.87	0.21	3.1
T2-BODIPY-589	580 ± 30 nm/460 ± 30 nm	15.3	1.32	-0.78	0.73	0.62	7.6
	610 ± 30 nm/460 ± 30 nm	21.2	0.94	1.26	0.46	0.79	17
	610 nm LP/460 ± 30 nm	151	8.09	1.44	1.89	0.80	15
	640 ± 30 nm/460 ± 30 nm	5.42	0.38	0.36	0.32	0.58	7.7

[a] The optimization results of the Nano Bioluminescent Resonance Energy Transfer (NanoBRET) assay conducted at a probe concentration of 1 µM. The table presents the mean and standard deviation of the maximum signal and background for each fluorescent tracer, along with the calculated Z' factor and signal window (SD) for various monochromatic conditions. A 610 nm long-pass filter was employed to optimize a single condition for each tracer.

Table 5. Evaluation of RIPK1 Unlabeled T2 Inhibitor Binding Affinities in NanoBRET Assay with Variable Monochromatic and Filter Conditions

Probes	*Monochromatic Settings with Selected Filter*	*T2 Inhibitor Ki (nM)*
T2-BODIPY-FL	520 ± 30 nm/460 ± 30 nm	14 ± 2.5
T2-BODIPY-FL	550 ± 30 nm/460 ± 30 nm	13 ± 3.4
T2-BODIPY-FL	580 ± 30 nm/460 ± 30 nm	9.1 ± 4.2
T2-BODIPY-589	610 ± 30 nm/460 ± 30 nm	6.6 ± 1.6
T2-BODIPY-589	610 nm LP/460 ± 30 nm	10 ± 1.5
T2-BODIPY-589	640 ± 30 nm/460 ± 30 nm	11 ± 2.8

List of Figures

Figure 1. TR-FRET and NanoBRET Assays for Evaluating RIPK1 Target Engagement 22
Figure 2. Validation of Tracer Compatibility for Enhanced TR-FRET Assay Performance 23
Figure 3. Dose-Response Titration of Unlabeled T2 Inhibitor with hRIPK1 Using Fluorescent Tracers to Assess Binding Interactions in TR-FRET assay 24
Figure 4. Validation of Tracer Compatibility for Enhanced NanoBRET Assay Performance 25
Figure 5. Assessment of Intracellular hRIPK1 Target Engagement of Unlabeled T2 Inhibitor Using NanoBRET Displacement Assay with Fluorescent Tracers 26

Figure 1. TR-FRET and NanoBRET Assays for Evaluating RIPK1 Target Engagement

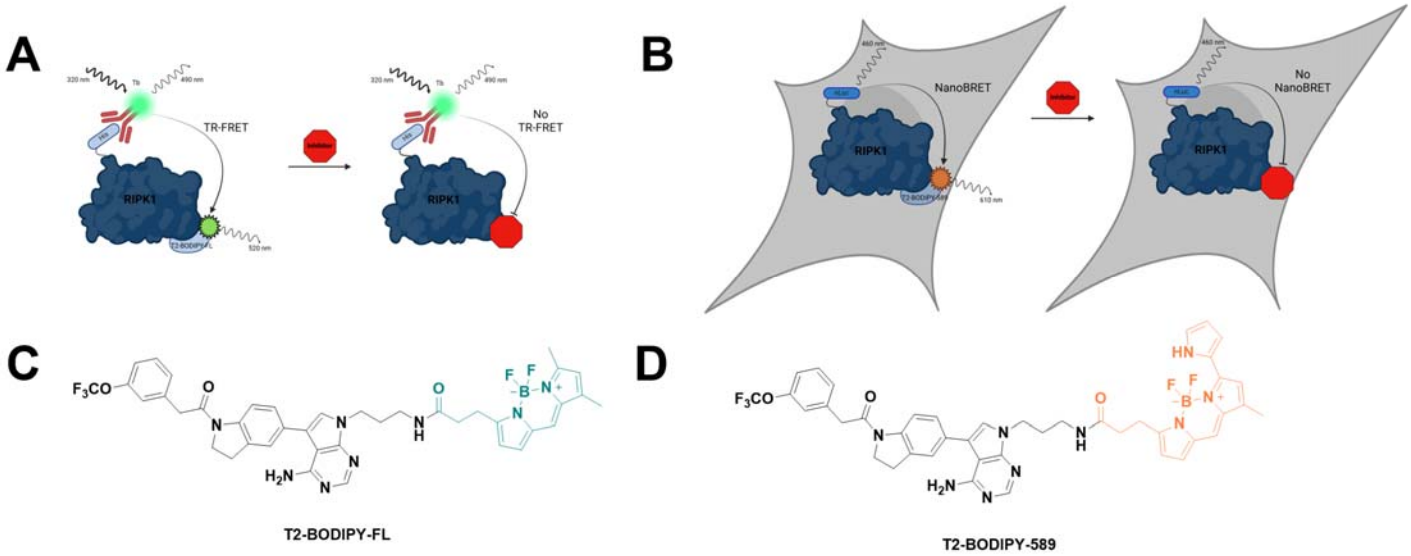

Figure 1. TR-FRET and NanoBRET Assays for Evaluating RIPK1 Target Engagement. (A) Schematic representation of the TR-FRET assay, illustrating the binding of anti-His-Tb antibody to His-tagged hRIPK1, which generates a specific TR-FRET signal in the presence of the fluorescent tracer T2-BDP-FL. This signal can be diminished by the addition of an unlabeled RIPK1 inhibitor. (B) Schematic depicting the expression of nLuc-hRIPK1 within the cell, resulting in a luminescent signal that is detected using the fluorescent tracer T2-BDP-589. This luminescent signal can be displaced by an unlabeled RIPK1 inhibitor. (C) Chemical structure of the T2-BDP-FL tracer utilized in this study. (D) Chemical structure of the T2-BDP-589 tracer utilized in this study.

Figure 2. Validation of Tracer Compatibility for Enhanced TR-FRET Assay Performance

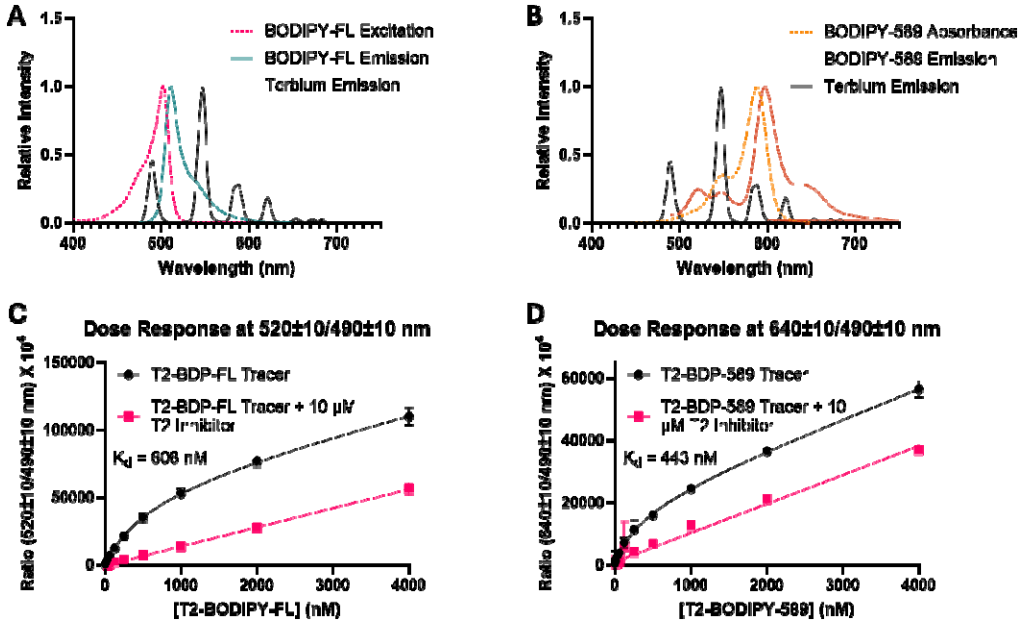

Figure 2. Validation of Tracer Compatibility for Enhanced TR-FRET Assay Performance. (A) Spectral overlap of Terbium (Tb) emission (black solid line) with the excitation spectrum of BODIPY-FL (red dashed line) and the emission spectrum of BODIPY-FL (green solid line). (B) Absorption (orange dashed line) and emission (red solid line) spectra of BODIPY-589, demonstrating overlap with Tb emission (black solid line). (C) Binding and nonspecific binding interactions of T2-BODIPY-FL in the presence of 1 nM His-hRIPK1 enzyme during the TR-FRET assay. (D) The total and nonspecific binding of T2-BODIPY-589 with 1 nM His-hRIPK1 enzyme in the TR-FRET assay, illustrating the effect of varying concentrations on binding efficacy. Data in C & D are presented as mean ± SEM (n=6 technical replicates).

Figure 3. Dose-Response Titration of Unlabeled T2 Inhibitor with hRIPK1 Using Fluorescent Tracers to Assess Binding Interactions in TR-FRET assay

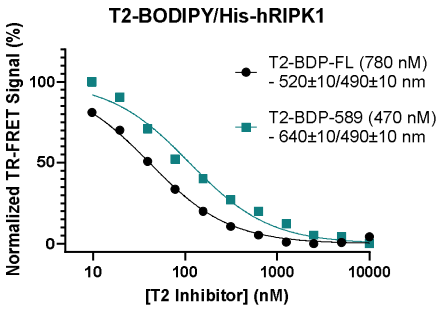

Figure 3. Dose-Response Titration of Unlabeled T2 Inhibitor with hRIPK1 Using Fluorescent Tracers to Assess Binding Interactions in TR-FRET assay. Dose-response titration of unlabeled T2 inhibitor with human RIPK1 using T2-BODIPY-FL and T2-BDP-589 as fluorescent tracers. The assay was performed with His tagged hRIPK demonstrating the predicted binding interactions. Data are presented as mean ± SEM (n=6 technical replicates).

Figure 4. Validation of Tracer Compatibility for Enhanced NanoBRET Assay Performance

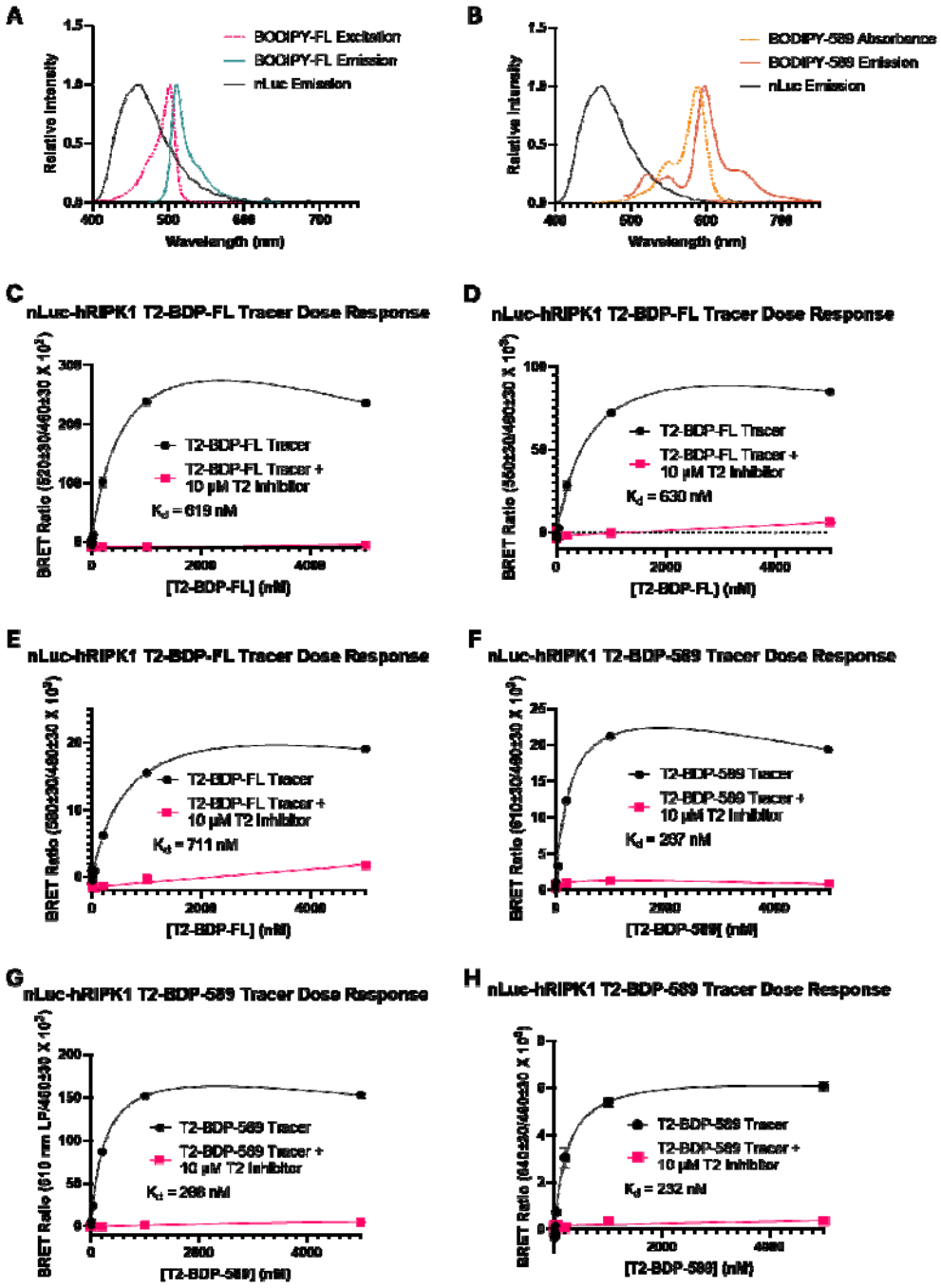

Figure 4. Validation of Tracer Compatibility for Enhanced NanoBRET Assay Performance. (A) Spectral overlap of nanoLuciferase (nLuc) emission (black solid line) with the excitation spectrum of BODIPY-FL (red dashed line) and the emission spectrum of BODIPY-FL (green solid line). (B) Absorption (orange dashed line) and emission (red solid line) spectra of BODIPY-589, demonstrating overlap with nLuc emission (black solid line). (C–E) Binding and nonspecific binding interactions of T2-BODIPY-FL to nLuc-hRIPK1 in HEK293T cells under different filter settings: 520 ± 30/460 ± 30 nm (C), 550 ± 30/460 ± 30 nm (D), and 580 ± 30/460 ± 30 nm (E). (F–H) Total and nonspecific binding of T2-BODIPY-589 to nLuc-hRIPK1 in HEK293T cells with filter settings of 610 ± 30/460 ± 30 nm (F), LP 610/460 ± 30 nm (G), and 640 ± 30/460 ± 30 nm (H), illustrating the effect of varying concentrations on binding efficacy. Data in C–H are presented as mean ± SEM (n = 4 technical replicates).

Figure 5. Assessment of Intracellular hRIPK1 Target Engagement of Unlabeled T2 Inhibitor Using NanoBRET Displacement Assay with Fluorescent Tracers

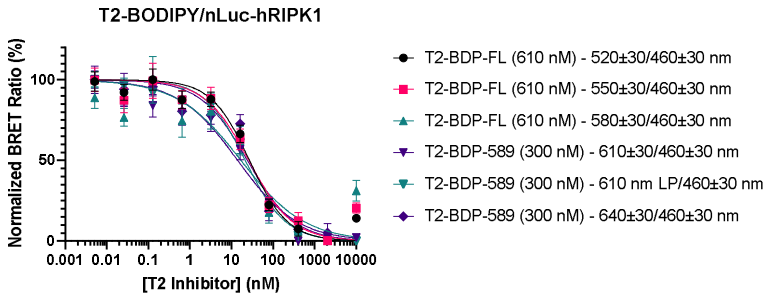

Figure 5. Assessment of Intracellular hRIPK1 Target Engagement of Unlabeled T2 Inhibitor Using NanoBRET Displacement Assay with Fluorescent Tracers. Dose-response titration of unlabeled T2 inhibitor with transiently transfected nLuc-hRIPK1 in HEK293T using T2-BODIPY-FL and T2-BDP-589 as fluorescent tracers. Data are presented as mean ± SEM (n=4 technical replicates).